JOURNAL OF CATALYSIS 153, 165–176 (1995)

Titania–Silica Mixed Oxides

I. Influence of Sol–Gel and Drying Conditions on Structural Properties

D. C. M. Dutoit, M. Schneider, and A. Baiker[1]

Department of Chemical Engineering and Industrial Chemistry, Swiss Federal Institute of Technology, ETH-Zentrum, CH-8092 Zurich, Switzerland

Received September 23, 1994; revised December 1, 1994

Mesoporous titania–silica aerogels with highly dispersed titanium have been prepared by an alkoxide-sol-gel process with ensuing semicontinuous extraction using supercritical CO_2. An acidic hydrolysant was added to a solution of tetraisopropoxytitanium(IV) modified by acetylacetonate and tetramethoxysilicon(IV) in isopropanol. The resulting titania–silica gels were dried by different methods, including conventional drying, high-temperature supercritical drying, and extraction with supercritical CO_2 (low-temperature aerogel). The influence of preparation parameters (the hydrolysis route, Ti-content, drying method, and calcination temperature) on the structural and chemical properties of the aero- and xerogels was studied by means of N_2-physisorption, X-ray diffraction, thermal analysis, and vibrational spectroscopy (FTIR, FTRaman). Prehydrolysis of the silicon alkoxide generally led to lower porosity, but did not influence the Si–O–Ti connectivity up to a calcination temperature of 1073 K. The conventionally dried xerogels contained titanium well-dispersed in the silica matrix and were predominantly microporous. High-temperature supercritical drying afforded meso- to macroporous aerogels with negligible microporosity, but undesired segregation of anatase. With the low-temperature aerogels, an increase of the nominal TiO_2 content from 2 to 20 wt% resulted in lower microporosity, higher BET surface area (up to ca. 700 m^2/g), and a rise in the contribution of Si–O–Ti species. Concomitantly the Ti–O–Ti connectivity increased without any indication of long-range ordering from X-ray analysis. The low-temperature aerogel with 20 wt% TiO_2 combined mesoporosity with high Ti dispersion and structural stability up to 873 K in air, properties desirable for epoxidation of olefins.

INTRODUCTION

Binary solids of silica and titania are of great importance as glasses with low thermal expansion coefficient (1–4), catalyst supports (5–10), and catalysts (11–15). Several preparation procedures have been applied, including flame hydrolysis (2), zeolite production (11), impregnation (6, 8, 13, 16), precipitation (7, 9, 12, 17), and sol-gel methods based on alkoxides (3, 5, 10, 14, 15, 18, 19).

Recently atomically mixed titania–silica has gained marked commercial and academic interest due to its potential as oxidation catalysts (11, 14, 20). A versatile method for achieving intimate mixing is the solution-sol-gel (SSG) technique (21), which represents a highly controllable preparation route with inherent advantages such as molecular-scale mixing of the constituents, purity of the precursors, homogeneity of the sol-gel product (prominent isotropy), and the use of different wet-chemical preparation tailoring tools. The as-prepared SSG products can be dried by means of different drying methods (22, 23). Especially in the case of "conventional" drying (temperature and/or vacuum), different detrimental forces are active, causing differential macroscopic and microscopic shrinkage and consequently severe cracking of the tenuous sol-gel structure (24). Supercritical drying is a suitable procedure for reducing the differential capillary stresses which result in such drastic structural rearrangements. The present state of supercritical drying (SCD) can be divided into two categories: the high-temperature method (25, 26) and the low-temperature method (27–29). Both methods circumvent the capillary stress either by transferring the solvent into the supercritical state (high-temperature method) or by replacing the solvent with CO_2 (low-temperature method), so eliminating any liquid vapour interfaces inside the gel-network during the solvent removal. An important difference between these two basic routes resides in the markedly higher critical temperatures of the alcoholic solvents (T_c > ca. 510 K) (high-temperature method) compared to the fairly low critical temperature of CO_2 (T_c = 304 K) (low-temperature method). With titania–silica, for example, high-temperature SCD usually leads to segregation of anatase, whereas low-temperature SCD "preserves" the wet-chemical SSG-structure and thus intimate mixing (22, 23).

[1] To whom correspondence should be addressed.

0021-9517/95 $6.00

The coupling of the sol-gel process with subsequent supercritical drying at low temperature offers a combination of the intrinsic advantages of the sol-gel method and the favourable textural characteristics of aerogels. Such a direct sol-gel preparation of a titania–silica with high dispersion and accessibility of the active surface fraction requires a careful control of the preparation conditions and knowledge of the sol-gel reactivity of the metal alkoxides used.

In general, the positive partial charge of titanium in the alkoxide precursor is significantly higher than that of silicon in the related alkoxide (30), which enhances the sol-gel activity of titanium over that of silicon (31, 32). This property often results in a "core-shell" structure, with titania forming the "cores" in this case. In addition, the homocondensation rate of $HO-Si(OR)_3$ species is significantly slower than the heterocondensation rate with $RO-Ti(OR)_3$ (33). Besides this behaviour, Basil and Lin showed that titanium tetraethoxide catalyzes the condensation of silanol groups (34–36).

To adjust the sol-gel reactivities of titanium and silicon alkoxide, two-stage hydrolysis was suggested by Yoldas (33). The silicon alkoxide is prehydrolyzed at a molar ratio of water to alkoxide (hydrolysis level), which is <4. Subsequently, the titanium alkoxide and the residual water for stoichiometric completion of the hydrolysis are added. The resulting mixed oxides with 25 wt% nominal TiO_2 are amorphous up to 1473 K. Aizawa *et al.* (31) investigated the influence of different preparation parameters (chelate ligands, pHs of hydrolysis, silicon alkoxides, and prehydrolysis) on the relative amount of heteronuclear Si–O–Ti connectivity by means of liquid attenuated total reflection FTIR spectroscopy. They reported (21) that for the chemical modification of titanium alkoxides with chelate ligands, an acidic medium, the use of tetramethoxysilicon(IV), and/or prehydrolysis are advantageous for producing intimately mixed titania–silica. The formation of titanium alkoxide chelates does not significantly influence the hydrolysis rate, but it lowers the functionality and thus the condensation rate of the hydrolyzed titanium species. In acidic medium the TiOH and SiOH groups are quite stable against ensuing homocondensation reactions [31, 37–39]. In addition, tetramethoxysilicon(IV) (TMOS) represents the most reactive silicon alkoxide (31, 40).

In the present study we have investigated systematically the influence of various preparation parameters (prehydrolysis, chemical composition, drying method, and calcination temperature) on the structural and chemical properties of titania–silica mixed oxides. The aim was to optimize these properties for titania–silica catalysts suitable for the catalytic epoxidation of olefins, which will be reported in part II of this series [41]. Vibrational spectroscopies (FTIR, FTRaman), X-ray diffraction, thermal analysis, and nitrogen physisorption were used for characterizing the titania–silica mixed oxides.

METHODS

Preparation Procedures

The wet-chemical preparation procedure used was based on the findings of Aizawa *et al.* (31) and Yoldas (33) concerning sol-gel reactivities, mentioned in the Introduction.

Throughout this work a set of acronyms is used, taking 10LTp as an example. The first numeral displays the nominal Ti content in weight percentage, based on the theoretical system TiO_2–SiO_2 (2 wt% "TiO_2" → 1.5 at% Ti; 5 wt% → 3.8 at%; 10 wt% → 7.7 at%; 20 wt% → 15.8 at%); the subsequent two capital letters represent the drying method used (low-temperature supercritical drying → LT; high-temperature supercritical drying → HT; Xerogel → X); and p stands for prehydrolysis.

Chemical modification of tetraisopropoxytitanium (IV). The modified titanium alkoxide precursor was synthesized according to the procedure described in detail in Ref. (31). In brief, two solutions were prepared. The first solution consisted of 10.01 g acetylacetone (*acac*) in 10 ml isopropanol (*i*-PrOH; Riedel-de Haen, extra pure) and the second of 28.4 g tetraisopropoxytitanium(IV) (TIPOT; Fluka, pract.) diluted in 30 ml *i*-PrOH (molar ratio TIPOT : *acac* = 1 : 1). The two solutions were mixed and refluxed for 1 h at 383 K under vigorous stirring (ca. 1000 rpm). After cooling the solution to ambient temperature, *i*-PrOH was evaporated at a reduced pressure of 10 kPa for 16 h. A yellow transparent liquid resulted, which still contained residual *i*-PrOH.

Sol-gel preparation. Quantities and conditions of the appropriate sol-gel preparations are listed in Table 1. In general, the sol-gel process was carried out in an antiadhesive, closed Teflon beaker (inner diameter 0.1 m), under nitrogen atmosphere, at ambient temperature (297 ± 2 K) and with a magnetic Teflon bead of 5 cm length. The total volume of the SSG sample was ca. 170 ml and the corresponding molar ratios H_2O : alkoxide : acid were 5 : 1 : 0.09.

In the *one-stage* synthesis route (*without prehydrolysis*), modified TIPOT and tetramethoxysilicon(IV) (TMOS; Fluka, puriss.) were dissolved in 22 ml *i*-PrOH. The hydrolysant consisted of doubly distilled water and hydrochloric acid (HCl 37 wt%; Fluka, puriss. p.a.) diluted in 15 ml *i*-PrOH. Via a dropping funnel the hydrolysant was added for 1 min to the alkoxide solution under vigorous stirring (ca. 1000 rpm) in a closed system, initially flushed with nitrogen. After 5 min, 84 ml *i*-PrOH was introduced.

With the *two-stage* preparation (*prehydrolysis*), the first

TABLE 1

Quantities, Composition, and Ageing Times of the Sol-Gel Preparations

Samples	TIPOT (mod.)[a] (mmol)	TMOS[b] (mmol)	HCl 37 wt% (mmol)	H_2O (mmol)	1. Ageing period[c] (h)	2. Ageing period[d] (h)	3. Ageing period[c] (h)	4. Ageing period[e] (h)
2LT	2.3	150	13.7	0.760	89	5[f]		
5LT	5.9	150	14.0	0.778	72	1	5[f]	15
5LTp	5.9	150	14.0	0.778	72	1	5[f]	15
10LT	12.5	150	14.6	0.811	15	1	20[f]	
10LTp	12.5	150	14.6	0.811	15	1	4[f]	
20LT	28.1	149.6	16.0	0.889	48[f]			
20LTp	28.1	149.6	16.0	0.889	48			72[f]
5HT	5.9	150	14.0	0.778	72	1	5[f]	15
10HT	12.5	150	14.6	0.811	15			
10X	12.5	150	14.6	0.811	72[f]			
10Xp	12.5	150	14.6	0.811	114[f]			

Note. Designations of the samples are explained under Methods.

[a] Tetraisopropoxytitanium(IV) complexed with acetylacetonate [TIPOT(mod.)].

[b] Tetramethoxysilicon(IV) (TMOS).

[c] Reduced stirring (ca. 500 ppm), nitrogen flow of 120 ml min^{-1}, and at ambient temperature.

[d] Reduced stirring, nitrogen flow, and at 333 K.

[e] Reduced stirring, hermetically closed, and at ambient temperature.

[f] Gelation of the SSG product within the appropriate ageing period.

solution consisted of TMOS dissolved in 22 ml *i*-PrOH and the second one (hydrolysant) of hydrochloric acid and doubly distilled water in 6 ml *i*-PrOH, leading to a hydrolysis level of 2. After homogenization of both solutions for 5 min, the hydrolysant was added to the TMOS solution via the dropping funnel and vigorously stirred for 45 min at 323 K (prehydrolysis of TMOS). After cooling the solution to ambient temperature, the modified TIPOT (prepared as described above) was added under vigorous stirring. 10 min later "completion" of the hydrolysis was achieved by addition of the residual amount of water (Table 1) diluted in 9.5 ml *i*-PrOH (via the dropping funnel, under vigorous stirring). Finally, 84 ml *i*-PrOH was introduced after another 5 min had elapsed. The different ageing procedures are summarized in Table 1.

Drying of the sol-gel product. Three different drying methods were applied.

(i) Conventional drying (xerogels): The titania–silica gel was dried at a pressure of 10 kPa and a temperature of 313 K for 22 h and at 373 K for another 24 h.

(ii) High-temperature supercritical drying (high-temperature aerogels): To exceed the critical conditions without formation of a vapour–liquid interface inside the pores (24), the SSG product, as described in Table 1 (5HT gel, 10HT sol), was transferred in a stainless steel liner into an autoclave with a net volume of 1.09 dm^3. In the case of 5HT, 170 ml of extra *i*-PrOH was added to cover the gel with solvent. The corresponding critical data for *i*-PrOH, the dominating component of all SSG solvents used in this work, are V_c = 220 ml mol^{-1}, T_c = 508 K, and p_c = 4.8 MPa (42). The high-pressure system was flushed with nitrogen, pressurised to 10 MPa, hermetically closed and heated at 1 K min^{-1} to 533 K. The autoclave was kept at the final temperature for 30 min to ensure complete thermal equilibration. The final pressure was ca. 23 MPa. The pressure was then isothermally released at 0.1 MPa min^{-1}. Finally, the system was flushed with nitrogen and allowed to cool to ambient temperature. The resulting beige aerogel clumps were ground in a mortar.

(iii) Semicontinuous extraction with supercritical carbon dioxide (low-temperature aerogels): To minimize flushing out of the wet-chemical SSG product, titania–silica gels were transferred into an autoclave with a net volume of 2 dm^3. The sample was stirred by a turbine stirrer (ca. 60 rpm) to minimize temperature inhomogeneities during the whole extraction procedure and by-passing of the gel lumps. Within 1 h and at a temperature of 313 K, the autoclave was pressurized with supercritical CO_2 to 24 MPa and the liquid–gas separator to 1 MPa, which resulted in an overall amount of 2.3 kg CO_2. The solvent of the SSG product was semicontinuously extracted by a CO_2 flow of 20 g min^{-1} for 5 h (6 kg CO_2) at a temperature of 313 K. The pressure was then isothermally released at ca. 20 g min^{-1}. Finally, the system was allowed to cool to ambient temperature. The resulting aerogel clumps were ground in a mortar.

Calcination procedure. Portions of the uncalcined (raw) aerogel or xerogel powder were calcined in a tubular reactor with upward flow. The temperature given corresponded to the oven temperature. The sample amount was ca. 2 g in all cases. To remove most of the organic residues prior to calcination, all aerogel and xerogel samples were first pretreated in a nitrogen flow of 0.5 dm^3 min^{-1} for 1 h. They were heated at 5 K min^{-1} to either 473 K in the case of ensuing calcination at 473 K or 673 K with all other samples. After cooling to ca. 353 K, they were heated again at 5 K min^{-1} in air flowing at 0.5 dm^3 min^{-1} and kept for 5 h at 473, 673, 873, or 1073 K.

Composition analysis. The composition was generally calculated on the basis of the nominal amounts used (Table 1) and independently confirmed by inductively coupled plasma atomic emission spectroscopy (ICPAES) analysis.

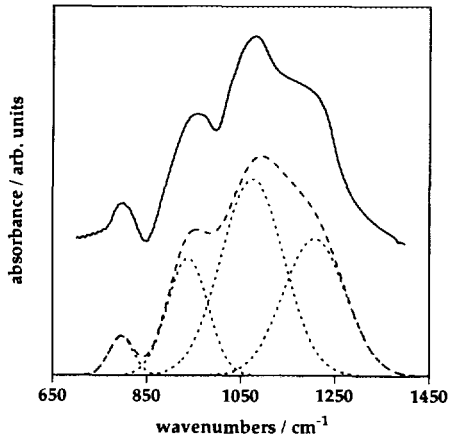

FIG. 1. Deconvolution of the FTIR spectrum of low-temperature aerogel 10LTp calcined in air at 873 K. (—) Original spectrum, (---) sum of the deconvoluted Gaussian curves, and (···) single Gaussian curves.

Physicochemical Characterization

Nitrogen physisorption. The specific surface areas (S_{BET}), mean cylindrical pore diameters ($\langle d_p \rangle$), and specific desorption pore volumes ($V_{p(N_2)}$) were determined by nitrogen physisorption at 77 K using a Micromeritics ASAP 2000 instrument. Note that $V_{p(N_2)}$ was assessed by the Barrett–Joyner–Halenda (BJH) method (43), which is assumed to cover the cumulative desorption pore volume of pores in the maximum range 1.7–300 nm diameter. Prior to measurement, the samples calcined at 473 and ≥673 K were degassed for 5 h at 423 and 473 K, respectively. The raw samples were degassed at 353 K for 16 h. The final pressure was ca. 0.1 Pa in the closed system for at least 1 min. BET surface areas were calculated in a relative pressure range between 0.05 and 0.2 assuming a cross-sectional area of 0.162 nm^2 for the nitrogen molecule. The pore size distributions were calculated applying the BJH method (43) to the desorption branches of the isotherms (44). The assessments of microporosity were made from *t*-plot constructions in the range $0.3 < t < 0.5$ nm, using the Harkins–Jura correlation (45).

X-ray diffraction. X-ray powder diffraction (XRD) patterns were measured on a Siemens θ/θ D5000 powder X-ray diffractometer. The diffractograms were recorded with Cu$K\alpha$ radiation over a 2θ-range of 10–80° or 15–40° in the case of poorly crystalline samples. The detector used was a scintillation counter with secondary monochromator. The mean crystallite sizes of anatase were determined from the Scherrer equation with the normal assumption of spherical crystallites (46) and the (200)-reflection (47), using the "Split Pearson7" fit-function.

FTIR spectroscopy. FTIR measurements were performed on a Perkin–Elmer series 2000 instrument. Sample wafers consisted of 105 mg dry KBr and ca. 1 mg sample. The sample cell was purged with a small flow of oxygen during the measurements. 200 scans were accumulated for each spectrum in transmission, at a spectral resolution of 4 cm^{-1}. The spectrum of dry KBr was taken for background substraction.

The FTIR spectra of titania–silica mixed oxides are characterized by a typical band assigned to framework titanium (48–50), which is usually quoted for the semi-quantitative estimate of the Si–O–Ti connectivity (11). This band was found at ca. 960 cm^{-1} for titanium-substituted silicalite zeolite [11], at 950 cm^{-1} (39), 945 cm^{-1} (51), and 940 cm^{-1} (52) for titania–silica xerogels, and at 940–950 cm^{-1} for aero- and xerogels (23).

For the evaluation of the FTIR results four bands were deconvoluted into Gauss curves, which is illustrated in Fig. 1. The positions and the assignments of these vibrations are as follows: (i) 800 cm^{-1} (21, 53), 810 cm^{-1} (39) for symmetric ν(Si–O–Si) stretching vibration; (ii) 940–960 cm^{-1} assumed for ν(Si–O–Ti) vibration (see above); (iii) 1080 cm^{-1} (21), 1095 cm^{-1} (39), 1080–1105 cm^{-1} (53) for asymmetric ν(Si–O–Si) stretching vibration; (iv) 1180 cm^{-1} (39), 1200 cm^{-1} (53), 1220 cm^{-1} (21) for asymmetric ν(Si–O–Si) stretching vibration.

For the deconvolution the starting values were chosen at 800, 950, 1080, and 1220 cm^{-1}, respectively, and the peak positions were not fixed. The peak shapes were optimized by applying the method of least mean square deviation (Fig. 1). The deconvoluted band positions of the calcined aerogels were in the range 780–807 cm^{-1}, 930–939 cm^{-1}, 1068–1090 cm^{-1}, and 1203–1217 cm^{-1}, respectively. The estimate of Si–O–Ti connectivity (Ti dispersion), $D_{(Si-O-Ti)}$, is defined

$$D_{(Si-O-Ti)} = \frac{S_{(Si-O-Ti)}}{S_{(Si-O-Si)}} * \frac{x_{Si}}{x_{Ti}}. \quad [1]$$

$S_{(Si-O-Ti)}$ and $S_{(Si-O-Si)}$ are the deconvoluted peak areas of the ν(Si–O–Ti) band at ca. 940 cm^{-1} and the ν(Si–O–Si) band at ca. 1210 cm^{-1}; x_{Si} and x_{Ti} designate the molar proportions of Si and Ti, respectively. Such $D_{(Si-O-Ti)}$ values are supposed to represent a semiquantitative measure of the proportion of Si–O–Ti species referred to the total Ti content and thus a kind of mixing efficiency or estimate of Ti dispersion.

To determine the experimental error of the FTIR evaluation, the preparation of the KBr wafer, the measurement of the spectrum, the deconvolution, and the evaluation based on Eq. [1] were repeated four times with 10LTp calcined at 873 K. The resulting standard deviation was ca. 3%. For the raw samples, the quality of deconvolution suffered from the presence of large amounts of organic residues, which caused a considerable background. In particular, with uncalcined samples the amount of organic residues was up to 10 wt% carbon determined by elemental microanalysis (Table 2).

FTRaman spectroscopy. For the Raman measurements the samples were transferred to 4-mm test tubes. Spectra were excited using the 1033-nm line of a YAG laser (Spectron Laser Systems). The back scattered light was analyzed by a Perkin–Elmer series 2000 instrument. With the high-temperature aerogel 1 W of power was focused on the sample, while for the low-temperature aerogel 2 W was used. The thus-induced temperatures of the samples were ca. 570 and 720 K, respectively. 7000 scans were accumulated for each spectrum, at a spectral resolution of 2 cm^{-1}.

Thermal analysis. TG investigations were performed on a Netzsch STA 409 instrument, coupled with a Balzers QMG 420 quadrupole mass spectrometer and equipped with Pt–Rh thermocouples and α-Al_2O_3 crucibles. A heating rate of 10 K min^{-1} and an air flow of 25 ml min^{-1} were used. The sample weight was ca. 100 mg and the α-Al_2O_3 reference weight ca. 80 mg.

Total carbon and hydrogen contents were determined with a LECO CHN-900 elemental microanalysis apparatus.

RESULTS

Structural and chemical properties of the aero(xero-) gels, both raw and calcined in air at different temperatures, are listed in Table 2.

Nitrogen physisorption

In general, the aerogels showed a type-IV isotherm with a type-H1 desorption hysteresis according to IUPAC classification (54) and mesoporosity with graphically determined maxima of the pore size distribution in the range 20–70 nm. As a typical example the adsorption/desorption isotherms, pore size distribution, and *t*-plot analysis of a portion of the low-temperature aerogel 20LT calcined at 673 K are depicted in Fig. 2. Only the samples of 5LTp, prepared via prehydrolysis and calcined in air at 673 and 873 K, exhibited a type-II isotherm without desorption hysteresis (54), indicative of a dominating contribution of microporosity. After calcination in air at 673 K, the aerogels possessed BET surface areas in the range 480–683 $m^2\ g^{-1}$ (Table 2).

With both the one-stage and the two-stage (prehydrolysis) synthesis series of low-temperature aerogels (*nn*LT and *nn*LTp, respectively), an increase of the Ti content caused generally a significant drop of the microporosity and a concomitant rise in mesoporosity (Table 2). However, for the prehydrolysed aerogels, the effects of the Ti content on both the microporosity, estimated from the appropriate *t*-plot analysis, and the mesoporosity were much more pronounced than those for the aerogels prepared without prehydrolysis (one-stage). With increasing Ti content, the specific micropore surface areas of the two-stage and one-stage aerogel samples, calcined at 673 K, dropped from 323 and 208 $m^2\ g^{-1}$ to 114 and 83 $m^2\ g^{-1}$, and the specific nitrogen pore volume developed from 0.14 and 0.99 $cm^3\ g^{-1}$ to 1.9 and 1.5 $cm^3\ g^{-1}$, respectively. The same tendencies became apparent for the corresponding samples calcined at 873 K. The textural properties of the xerogel series 10X and 10Xp and those of the high-temperature aerogel series 5HT and 10HT showed a comparable dependence on the hydrolysis procedure chosen and the Ti content, respectively (Table 2).

The pore size distributions, derived from the desorption branch of nitrogen physisorption, and the *t*-plots of differently dried titania–silica materials are shown in Fig. 3. When compared to the type-IV isotherms with type-H1 desorption hysteresis of both the high-temperature aerogel series 10HT and the low-temperature series 10LT, the samples of xerogel 10X calcined at 673 and 873 K reveal a type-I isotherm without desorption hysteresis (54), which indicates a dominating contribution of microporosity (Table 2). The graphically assessed pore-size maxima of the pore-size distributions derived from the desorption branches were in the range 20–70 nm for the aerogel samples (except for 5LTp, 1.5 nm) and 1.5 nm for the xerogels. A comparison of differently dried samples calcined in air at 673 K provides the following order of decreasing mesoporosity and simultaneously increasing microporosity (Table 2): high-temperature aerogel 10HT ($V_{p(N_2)}$ 3.6 $cm^2\ g^{-1}$, S_t 0 $m^2\ g^{-1}$), low-temperature aerogel 10LT ($V_{p(N_2)}$ 1.7 $cm^3\ g^{-1}$, S_t 140 $m^2\ g^{-1}$), and xerogel 10X ($V_{p(N_2)}$ 0.026 $cm^3\ g^{-1}$, S_t 407 $m^2\ g^{-1}$). The corresponding BET surface areas are 598, 683, and 473 $m^2\ g^{-1}$, respectively. Similar tendencies were found with the corresponding samples calcined in air at 873 K.

The influence of the calcination temperature is illus-

TABLE 2

Structural and Chemical Properties of the Aero(Xero-)Gels Both Raw and Calcined in Air at Different Temperatures

Sample	Calc. (K)	S_{BET} (S_t) (m^2/g)[a]	$V_{p(N2)}$ (cm^3/g)[b]	$\langle d_p \rangle$ (nm)[c]	$S_{(Si-O-Ti)}/S_{(Si-O-Si)}$[d]	$D_{(Si-O-Ti)}$[e]	C-content (%)
2LT	—	—	—	—	—	—	6.2
	673	497(355)	0.28	2(70)	0.26	17	—
	873	410(292)	0.39	4(60)	0.26	17	—
5LT	—	—	—	—	—	—	10.7
	673	518(208)	0.99	8(40)	—	—	—
	873	489(212)	1.0	8(40)	0.38	9.5	—
5LTp	—	—	—	—	—	—	12.4
	673	480(323)	0.14	1.2(1.5)	—	—	—
	873	381(254)	0.11	1.2(1.5)	0.45	11.5	—
10LT	—	603(102)	2.0	13(55)	0.52	6.3	9.3
	473	634(139)	1.7	11(55)	0.55	6.6	3.1
	673	683(140)	1.7	10(55)	0.49	5.9	0.2
	873	557(98)	1.4	10(50)	0.50	6.0	<0.1
	1073	463(35)	1.7	14(50)	0.47	5.6	<0.1
10LTp	—	458(127)	0.69	6(40)	0.52	6.2	11.3
	473	483(182)	0.73	6(60)	0.55	6.6	5.2
	673	533(214)	1.2	9(60)	0.50	6.0	0.2
	873	433(145)	1.1	10(50)	0.51	6.1	0.2
20LT	—	—	—	—	—	—	8.9
	673	674(83)	1.5	9(40)	—	—	—
	873	550(32)	1.3	10(40)	0.55	2.9	—
20LTp	—	—	—	—	—	—	11.2
	673	682(114)	1.9	11(30)	—	—	—
	873	508(79)	1.5	12(30)	0.57	3.0	—
5HT	—	—	—	—	—	—	5.2
	673	553(1)	2.7	19(20)	0.12	3.0	—
	873	568(0)	2.8	20(20)	0.09	2.2	—
10HT	—	—	—	—	0.12	1.5	3.5
	673	598(0)	3.6	24(60)	0.14	1.7	—
	873	611(0)	3.7	24(50)	0.12	1.4	—
10X	—	—	—	—	0.57	6.8	11.4
	673	473(407)	0.03	0.3(1.5)	—	—	—
	873	256(202)	0.02	0.3(1.5)	—	—	—
10Xp	—	—	—	—	0.59	7.1	12.5
	673	399(337)	0.02	0.2(1.5)	—	—	—
	873	176(114)	0.01	0.2(1.5)	—	—	—
Zeolite TS-1[f]	823	417(306)	0.50	5(45)	0.39	17	<0.1

Note. Designations of the samples are explained under Methods.

[a] (S_t), in parentheses, denotes specific micropore surface area derived from *t*-plot analysis.

[b] $V_{p(N_2)}$ designates the BJH cumulative desorption pore volume of pores in the maximum range 1.7–300 nm diameter.

[c] $\langle d_p \rangle = 4V_{p(N2)}/S_{BET}$; in parentheses, the graphically assessed pore-size maximum of the pore-size distribution derived from the desorption branch are given.

[d] Relative contribution of Si–O–Ti entities, estimated from the ratio of Si–O–Ti (930–939 cm^{-1}) and Si–O–Si (1205–1215 cm^{-1}) peak areas.

[e] $D_{(Si-O-Ti)}$; estimate of Ti dispersion derived from Eq. [1].

[f] Zeolite TS-1 (3.1 wt% "TiO_2" → 2.3 at% Ti) given for comparison.

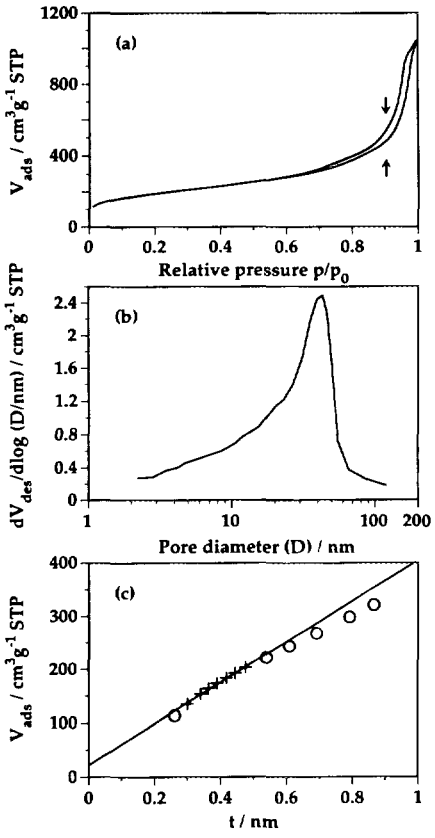

FIG. 2. Nitrogen physisorption (77 K) on aerogel 20LT calcined at 673 K in air. (a) Adsorption(↑)/desorption(↓) isotherms (STP; 273.15 K, 1atm), (b) pore-size distribution derived from the desorption branch of nitrogen physisorption, and (c) *t*-plot analysis ((+) points taken for linear regression). Designations of samples are explained under Methods.

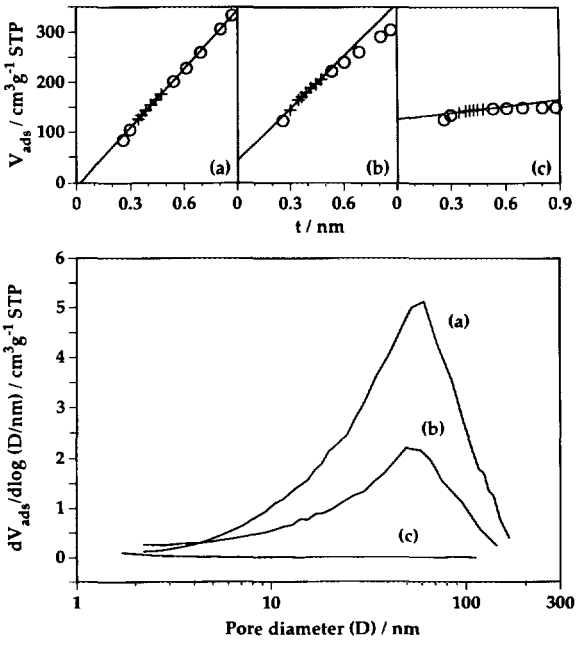

FIG. 3. Textural properties of differently dried samples, all calcined in air at 673 K and with 10 wt% nominal TiO_2. (a) High-temperature aerogel 10HT, (b) low-temperature aerogel 10LT, and (c) xerogel 10X. Bottom: differential pore-size distributions derived from the desorption branches of the physisorption isotherms; top: *t*-plot presentation ((+) points taken for linear regression).

trated by the 10LT and 10LTp series (Table 2). Note that a rise in temperature to 673 K caused an increase of the BET surface area from 603 to 683 $m^2\ g^{-1}$ and from 458 to 533 $m^2\ g^{-1}$, respectively. However, at higher temperatures a significant decline in the BET surface areas was observed with both series. The BET surface areas of the high-temperature aerogel series, 5HT and 10HT, were almost independent of the calcination temperature up to 873 K (Table 2).

X-Ray Diffraction

X-ray analysis indicated that all low-temperature aerogels as well as xerogels were X-ray amorphous at temperatures ≤873 K. Aerogel 10LT was even amorphous up to 1073 K. On the contrary, the high-temperature aerogels 5HT and 10HT, both raw and calcined in air at temperatures ≤873 K, contained well-developed anatase crystallites ($\langle d_c \rangle$ ca. 8 nm) which remained almost unchanged up to 873 K.

The effect of the drying method applied on the structure of the titania–silica, as revealed by X-ray diffraction, is illustrated in Fig. 4. X-ray diffraction patterns of the uncalcined xerogel 10X, the low-temperature aerogel 10LT, and the high-temperature aerogel 10HT are compared.

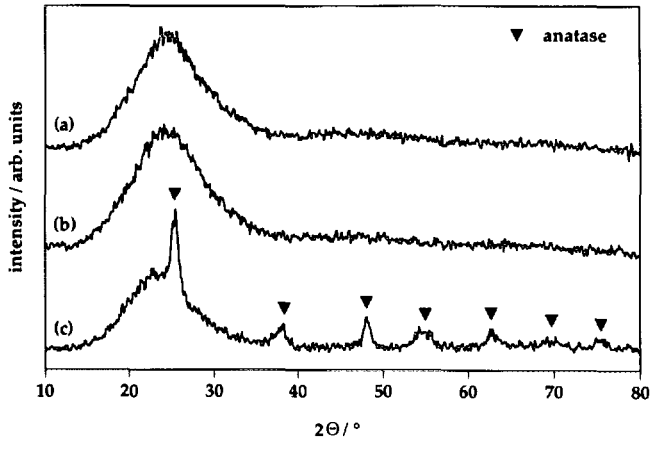

FIG. 4. X-ray diffraction patterns (Cu$K\alpha$) of (a) xerogel 10X, (b) low-temperature aerogel 10LT, and (c) high-temperature aerogel 10HT. All samples are uncalcined and with 10 wt% nominal TiO_2. Designations of samples are explained under Methods. (▼) Anatase.

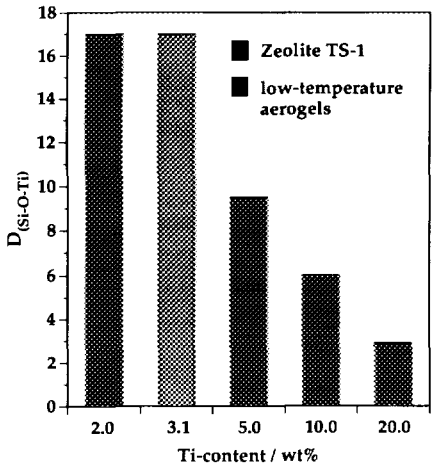

FIG. 5. Influence of the Ti content on the normalized Si–O–Ti connectivity ($D_{(Si-O-Ti)}$, defined in Eq. [1]) of the low-temperature aerogels prepared via one-stage hydrolysis and calcined in air at 873 K. Values for zeolite TS-1 are given for comparison.

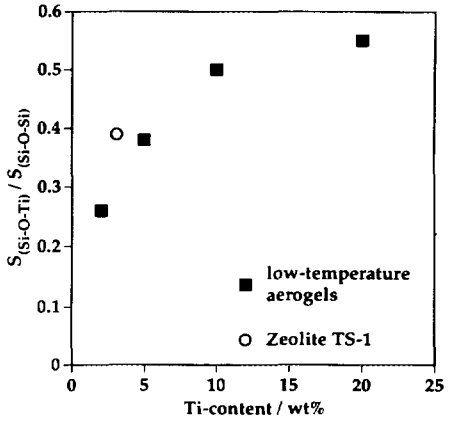

FIG. 6. Influence of the Ti content on the contribution of Si–O–Ti species estimated from the ratio $S_{(Si-O-Ti)}/S_{(Si-O-Si)}$ (derived from FTIR measurements) of the low-temperature aerogels prepared via one-stage hydrolysis and calcined in air at 873 K. $S_{(Si-O-Ti)}$ and $S_{(Si-O-Si)}$ represent the peak areas of the Si–O–Ti band at ca. 940 cm^{-1} and the Si–O–Si band at ca. 1210 cm^{-1}, respectively. The corresponding property for zeolite TS-1 is given for comparison.

FTIR Spectroscopy

As an estimate for the abundancy of Si–O–Ti entities in the mixed oxide, the ratio of the deconvoluted peak areas $S_{(Si-O-Ti)}/S_{(Si-O-Si)}$ and its normalized $D_{(Si-O-Ti)}$ value, defined in Eq. [1], were used (Table 2). The Si–O–Ti connectivity $D_{(Si-O-Ti)}$ is assumed to represent a relative measure of the proportion of Si–O–Ti species referred to the total Ti-content and thus provide a kind of mixing efficiency, a quantity related to Ti-dispersion (see Experimental).

With respect to the influence of prehydrolysis (two-stage) similar values for the Si–O–Ti connectivity were obtained with both hydrolysis routes at equal Ti contents. Thus, prehydrolysis did not significantly affect Si–O–Ti connectivity, as determined by FTIR.

The effect of the Ti content is displayed in Figs. 5 and 6 for the low-temperature aerogels *nn*LT calcined at 873 K and compared with the zeolite TS-1 (3.1 wt% "TiO_2" → 2.3 at% Ti) (20), which is considered to possess optimum Ti dispersion. An increase of the Ti content caused a distinct decrease of $D_{(Si-O-Ti)}$ (Fig. 5). Note, however, that the contribution of Si–O–Ti species expressed as $S_{(Si-O-Ti)}/S_{(Si-O-Si)}$ increased significantly up to 20 wt% TiO_2 as illustrated in Fig. 6.

FTIR spectra of the differently dried, uncalcined samples with 10 wt% nominal TiO_2 are presented in Fig. 7. The band at ca. 950 cm^{-1}, indicative of Si–O–Ti species, is well-developed with both the low-temperature aerogel 10LT and the xerogel 10X, but only weak for the high-temperature aerogel 10HT. Accordingly, it seems that both the low-temperature aerogel and the xerogel possess significantly higher Ti dispersions than the high-temperature aerogel, which is schematically shown in Fig. 8,. This finding is in agreement with the results from X-ray analysis (Fig. 4). A similar behaviour was observed with portions of the aerogels 5LT and 5HT, both calcined in air at 873 K and with 5 wt% nominal TiO_2.

As concerns the effect of calcination temperature, the $D_{(Si-O-Ti)}$ values (Table 2) of the 10LT and 10LTp series were almost independent of the calcination temperature up to 1073 and 873 K, respectively.

Raman spectroscopy

The influence of the drying method is also evident from the Raman spectra depicted in Fig. 9. With the high-

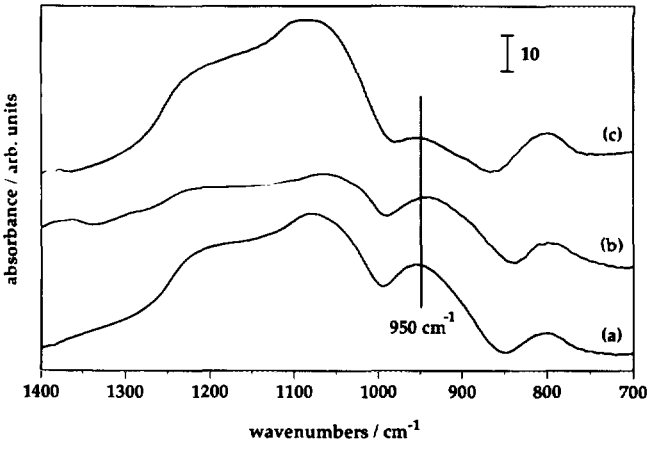

FIG. 7. FTIR spectra of (a) low-temperature aerogel 10LT, (b) xerogel 10X, and (c) high-temperature aerogel 10HT. All samples are uncalcined and with 10 wt% nominal TiO_2. Designations of samples are explained under Methods.

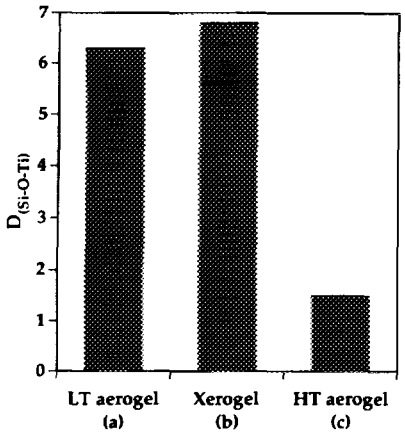

FIG. 8. Influence of the drying method on the normalized Si–O–Ti connectivity ($D_{(Si-O-Ti)}$, defined in Eq. [1]). (a) Low-temperature aerogel 10LT, (b) xerogel 10X, (c) high-temperature aerogel 10HT. All samples are uncalcined and with 10 wt% nominal TiO_2.

temperature aerogel 10HT, calcined in air at 873 K, the presence of crystalline anatase is independently confirmed by the corresponding lattice vibrations at 393, 515, and 638 cm^{-1} (22). In contrast, the low-temperature aerogel 10LT, calcined in air at 873 K, shows bands at 952 and 1100 cm^{-1} which are both assigned to ν(Si–O–Ti) vibrations (21). The band at 1100 cm^{-1}, however, is superimposed by the asymmetric ν(Si–O–Si) stretching vibration at 1070 cm^{-1} (21). The bands at 430, 488, 605, and 800 cm^{-1} are also found in pure silica xerogels (55). The very broad band at 430 cm^{-1} is assigned to Si–O–Si bending modes, and the bands at 488 and 605 cm^{-1} are attributed to defects in the network. Best and Condrate (50) attribute the broadening of the 430 cm^{-1} band with increasing Ti content in titania–silica systems to greater

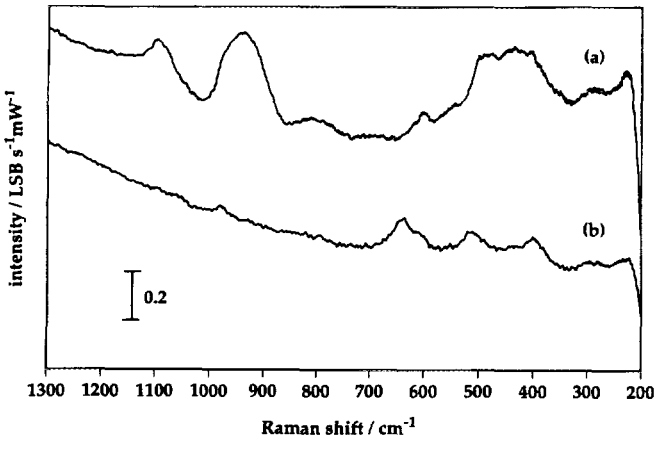

FIG. 9. Raman spectra of (a) low-temperature aerogel 10LT and (b) high-temperature aerogel 10HT. Both aerogels are with 10 wt% nominal TiO_2 and calcined in air at 873 K.

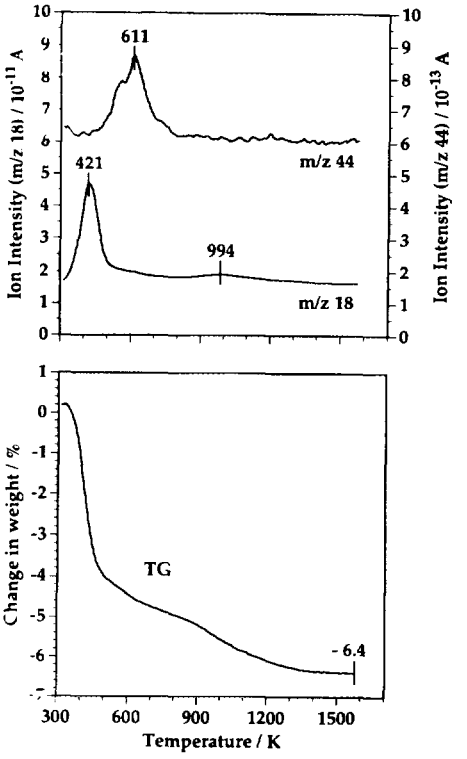

FIG. 10. Thermoanalytical investigation of prehydrolyzed low-temperature aerogel 10LTp calcined in air at 873 K. Bottom: TG curve; top: ion intensities of $m/z(CO_2^+)$ = 44 (CO_2) and $m/z(H_2O^+)$ = 18 (H_2O). Heating rate: 10 K min^{-1}, air flow 25 ml min^{-1}.

incorporation of Ti into tetrahedral sites in the silica network with concomitant distortion of the SiO_4 tetrahedra (Fig. 9).

Thermal Analysis

Thermal analysis was performed in flowing air with a heating rate of 10 K min^{-1}. The thermoanalytical results of the prehydrolyzed 10LTp, calcined at 873 K, are presented in Fig. 10. The weight loss of the sample originated mainly from the evolution of water (desorption of physisorbed water, dehydroxylation), which was already present in the samples. This conclusion emerges from relating the TG curve to the monitored ion intensities of CO_2^+ (m/z = 44) and H_2O^+ (m/z = 18). The evolution of water began at room temperature and reached a prominent maximum at 421 K with an ensuing weak signal at 994 K (Fig. 10). The CO_2 evolution occurred at ca. 430 K and reached its maximum at 611 K. The weight loss up to a temperature of 1500 K amounted to 6.4 wt%.

All aero- and xerogels contained remarkable carbon contents, as deduced from elemental microanalysis. These organic residues are likely to originate from the realkoxylation of surface hydroxyl groups and the incor-

poration of both unhydrolyzed alkoxide ligands and acetylacetonate, as well as residual solvent in the SSG matrix (56). In terms of the hydrolysis route chosen, prehydrolysis generally led to higher amounts of organic residues. When compared to low-temperature aerogels and xerogels, the high-temperature aerogels possess distinctly smaller carbon contents, as shown in Table 2. With the one-stage samples loaded with 10 wt% nominal TiO_2, for example, the appropriate carbon contents were 9.3, 3.5, and 11.4 wt%, respectively. The relatively high values for the low-temperature aerogels and xerogels seem to be dominated by the contribution of residual alcoholic solvent, whereas the carbon contents of the high-temperature aerogels are mainly attributed to the realkoxylation of surface hydroxyl groups during high-temperature SCD (56). It emerges from the 10LT and 10LTp series that only calcination at temperatures up to 673 K reduces the amount of organic contaminants to $\leq$0.2 wt% carbon (Table 2).

DISCUSSION

Influence of Prehydrolysis and Ti Content

The textural properties of low-temperature aerogels indicate a marked dependence on the type of hydrolysis chosen. With prehydrolysis, the BET surface area and the mesoporosity decline, whereas the contribution of microporosity increases (Table 2). This effect is especially prominent with samples of low titania content. It seems that prehydrolysis favours the formation of "silica-like" polymeric species lending themselves to microporous structure. For titania–silica xerogels similar behaviour was observed by Handy *et al.* (18). The authors showed that prehydrolysis together with acid catalysis leads to the buildup of very tenuous wet-gel structures, which are highly susceptible to pore collapse during the drying process, resulting in considerable microporosity. In the case of semicontinuous extraction with supercritical CO_2, Rangarajan and Lira (57) showed that stresses within the gel-network due to adsorption during depressurization are most probably the reason for shrinkage. This finding might explain the large contribution of microporosity with prehydrolyzed low-temperature aerogels originating from tenuous gels susceptible to pore collapse (Table 2). The prehydrolysis step does not seem to influence the distribution and/or connectivity of Ti as judged from the FTIR analysis (Table 2). This is further supported by the fact that prehydrolysis did not lead to different results in the catalytic epoxidation of olefinic reactants, which will be reported in part II of this study (41).

An increase of the Ti content from 2 to 5 wt% nominal TiO_2 led to a rise in both BET surface area and mesoporosity, but to a concomitant decline of microporosity, which was independent of the hydrolysis route chosen (Table 2). The marked mesoporosity of especially the 20LT series, combined with its high thermal stability, renders these aerogels promising catalysts for use in liquid-phase oxidation. Wide pores make the large internal surface area accessible for bulky reactants, which is demonstrated by the excellent catalytic behaviour of these samples (41).

The investigation of the Si–O–Ti connectivity indicates highest $D_{(Si-O-Ti)}$ values for both the low-temperature aerogel with 2 wt% "TiO_2" (2LT) and the zeolite TS-1 with 3.1 wt% "TiO_2," quoted for comparison (Table 2, Fig. 5). If we assume that the zeolite TS-1 possesses an atomic distribution of the titanium ions in the silica matrix, we may conclude that only with the 2LT series, containing 2 wt% nominal TiO_2, similar dispersion has been achieved. With higher Ti content, the $D_{(Si-O-Ti)}$ values (Fig. 5) decrease, whereas the absolute contribution of ν(Si–O–Ti) vibrations ($S_{(Si-O-Ti)}/S_{(Si-O-Si)}$), depicted in Fig. 6, increases. This behaviour indicates that a rise of the Ti content favours the formation of Ti–O–Ti structural units, which even grow to titanium oxo nanodomains, as shown by UV–vis spectroscopy in part II (41). As regards the possible enrichment of the surface layers by titanium ions, estimates of the surface free energies of TiO_2 and SiO_2 (58) do not allow a reliable prediction of the behaviour of such highly mixed systems, especially not in the presence of organic contaminants.

Influence of the Drying Method

The lower surface areas and pore volumes of the xerogels can be explained by the occurrence of differential capillary forces in the gel-network during the drying procedure (Table 2). The prominent meso- to macroporosity of the high-temperature aerogels is very likely a result of the increased water reactivity under the conditions applied during high-temperature SCD (533 K). On a molecular scale especially water can cause dissolution, reprecipitation, depolymerization, repolymerization, alkoxylation, and enhanced syneresis (network densification) leading to chemical and/or restructuring phenomena in these materials (56, 59). Such processes include Ostwald ripening, coalescence–coarsening, sintering, and syneresis resulting in larger pore volumes. With the aerogels obtained by semicontinuously extracting with supercritical CO_2 at 313 K, it is supposed that stresses within the gel-network due to adsorption during depressurization are the most probable cause for shrinkage (57).

The large influence of the drying method used on the estimated Si–O–Ti connectivity ($D_{(Si-O-Ti)}$) may be inferred from the structural properties of TiO_2 and SiO_2. The average bond angles are 159° with Ti–O–Ti and 152° with Si–O–Si; the average bond lengths are 1.80–1.86 Å for Ti–O and 1.6 Å for Si–O. These similar structural

properties are suggested to allow substitution of Si for Ti in a silica matrix (60). The experimentally determined crystallization temperature on heating (T_{ch}) compared with the adiabatic nucleation temperature (T_{14}) is used to classify the glass-forming properties of oxides (61, 62). Accordingly, SiO_2 represents a good glass former ($T_{ch} > T_{14}$), whereas TiO_2 has comparably poor glass forming properties ($T_{ch} < T_{14}$). This restriction of amorphicity (glass forming properties) with TiO_2 is considered to be a decisive factor, limiting the complete miscibility of titanium ions in the silica matrix. The wet gels are assumed to be free of extensive Ti–O–Ti connectivity, but are shown to contain Si–O–Ti groups (31). With the high-temperature aerogels, the SSG products were exposed to a temperature of 533 K during SCD. This high temperature is apparently sufficient to transform the structure of the SSG system into a thermodynamically stabilized state, consisting of silica and titania agglomerates. The processes concerned have already been mentioned above. In contrast, the highly dispersed state of the SSG system could be preserved with both the low-temperature aerogels extracted at 313 K and the xerogels dried at 373 K, probably due to the fact the thermodynamic stabilization is kinetically hindered (56, 59).

A similar dependence of the Ti dispersion on the drying method used was reported by Cogliati *et al.* (22) and Beghi *et al.* (23). The exposure to elevated temperatures during the high-temperature SCD led to crystallization of anatase, whereas gels dried at low temperature (xerogels and low-temperature aerogels) were X-ray amorphous, after calcination up to 1473 K, and Ti contents of 10 wt% nominal TiO_2. Bräutigam *et al.* [52] studied the structural changes during the gel-to-oxide transformation of sol-gel derived samples using FTIR spectroscopy. They suggested that Si–O–Ti interactions concentrate at the boundaries of the silica and titania phases. Thus, the contribution of Si–O–Ti species is considered to be correlated with the size of titania and silica agglomerates. A similar behaviour emerges from the results of X-ray analysis (Fig. 4, Table 2) and vibrational spectroscopy (Fig. 9, Table 2). This model is further supported by the XPS studies presented by Ingo et al. (63).

Effects of the Calcination Temperature

The increase of the BET surface area, after calcination in air at 673 K, is a result of the removal of organic residues, rendering the surface accessible for the physisorption of nitrogen (64) (Table 2). The subsequent decrease at temperatures >673 K can result from processes such as Ostwald ripening, coalescence–coarsening, sintering, and syneresis.

The estimates of values for Si–O–Ti connectivity are virtually not influenced by the calcination temperature up to 873 K, and those for the 10LT series are virtually not influenced even up to 1073 K. This finding is consistent with the results from the X-ray diffraction analysis and in agreement with the phase diagram reported by Hayashi *et al.* (3) for titania–silica xerogels with Ti contents up to 30 wt% nominal TiO_2, calcined in air up to 1373 K.

CONCLUSIONS

Various drying methods have been used for the drying of alkoxide-sol-gel-derived titania–silica mixed oxides. Titania–silica aerogels combining mesoporosity and high dispersion of the Ti constituent could be prepared only by applying semicontinuous extraction of titania–silica alcogels with supercritical CO_2. FTIR spectroscopy has been used to gain information about the dispersion of the titania. The ratio of the band due to ν(Si–O–Ti) at ca. 940 cm^{-1} to that due to ν(Si–O–Si) at ca. 1210 cm^{-1} proved to be a useful measure for the Ti dispersion. The drying method and the Ti content were found to have a prominent influence on both the textural properties and the titania dispersion. The highest Ti dispersion, comparable with that of the zeolite TS-1, was determined for the low-temperature aerogel with 2 wt% of nominal TiO_2. The absolute contribution of Si–O–Ti species increased with a rise in Ti content, as indicated by the increasing ratio of the peak areas at 940 and 1210 cm^{-1}. Xerogels possessed high Ti dispersion, but were predominantly microporous. High-temperature SCD resulted in anatase segregation and marked meso- to macroporosity, which is attributed to the enhanced solvent reactivity at 533 K during SCD. Prehydrolysis of the silicon alkoxide generally led to lower porosity, but had no significant influence on Si–O–Ti connectivity up to a calcination temperature of 1073 K. Among the titania–silica mixed oxides prepared, the low-temperature aerogel with 20 wt% nominal TiO_2 possessed mesoporosity combined with high Ti dispersion and structural stability, rendering this aerogel most favourable for use in liquid-phase epoxidation, as will be reported in part II of this series [41].

ACKNOWLEDGMENTS

Thanks are due Reiner Glöckler and Professor Jens Weitkamp for providing the TS-1 sample. Financial support of this work by the "Kommission zur Förderung der Wissenschaftlichen Forschung" and F. HOFFMANN-LA ROCHE AG, Switzerland is gratefully acknowledged.

REFERENCES

1. Nordberg, M. E., U.S. Patent 2,326,059, August 3, 1943.
2. Schultz, P. C., *J. Am. Ceram. Soc.* **59,** 214 (1976).
3. Hayashi, T., Yamada, T., and Saito, H., *J. Mater. Sci.* **18,** 3137 (1983).

4. Deng, Z., Breval, E., and Pantano, C. G., *J. Non-Cryst. Solids* **100,** 364 (1988).
5. Baiker, A., Dollenmeier, P., Glinski, M., and Reller, A., *Appl. Catal.* **35,** 365 (1987).
6. Rajadhyaksha, R. A., and Knözinger, H., *Appl. Catal.* **51,** 81 (1989).
7. Vogt, E. T. C., Boot, A., van Dillen, A. J., Geus, J. W. Janssen, F. J. J. G., and van den Kerkhof, F. M. G., *J. Catal.* **114,** 313 (1988).
8. Rieck, J. S., and Bell, A. T., *J. Catal.* **99,** 262 (1986).
9. Ko, E. I., Chen, J.-P., and Weissmann, J. G., *J. Catal.* **105,** 511 (1987).
10. Cauqui, M. A., Calvino, J. J., Cifredo, G., Esquivias, L., and Rodriguez-Izquierdo, J. M., *J. Non-Cryst. Solids* **147&148,** 758 (1992).
11. Jacobs, P. A., *in* "Selective Oxidations in Petrochemistry, Tagungsbericht 9204, Proceedings of the DGMK-Conference, 1992, Goslar, Germany" (M. Baerns and J. Weitkamp, Eds.), p. 171. DGMK, Hamburg, 1992; references therein.
12. Imamura, S., Tarumoto, H., and Ishida, S., *Ind. Eng. Chem. Res.* **28,** 1449 (1989).
13. Niwa, M., Sago, M., Ando, H., and Murakami, Y., *J. Catal.* **69,** 69 (1981).
14. Neumann, R., Chava, M., and Levin, M., *J. Chem. Soc. Chem. Commun.*, 1685 (1993).
15. Moini, A., U.S. Patent 5,162,283, November 10, 1992.
16. Fernandez, A., Leyrer, J., Gonzalez-Elipe, A. R. Munuera, G., and Knözinger, H., *J. Catal.* **112,** 489 (1988).
17. Shikada, T., Fujimoto, K., Kunugi, T., and Tominaga, H., *Ind. Eng. Chem. Prod. Res. Dev.* **20,** 91 (1981).
18. Handy, B. E., Maciejewski, M., Baiker, A., and Wokaun, A., *J. Mater. Chem.* **2**(8), 833 (1992).
19. Yuan, L., Yao, G., *J. Non-Cryst. Solids* **100,** 309 (1988).
20. Notari, B., *Catal. Today* **18,** 163 (1993).
21. Brinker, C. J., and Scherer, G. W., "Sol-Gel Science, the Physics and Chemistry of Sol-Gel Processing." Academic Press, San Diego, 1990.
22. Cogliati, G., Guglielmi, M., Che, T. M., and Clark, T. J., *Mater. Res. Soc. Symp. Proc.* **180,** 329 (1990).
23. Beghi, M., Chiurlo, P., Costa, L., Palladino, M., and Pirini, M. F., *J. Non-Cryst. Solids* **145,** 175 (1992).
24. Scherer, G. W., *J. Am. Ceram. Soc.* **73,** 3 (1990).
25. Kistler, S. S., *J. Phys. Chem.* **36,** 52 (1932).
26. Nicolaon, G. A., and Teichner, S. J., *Bull. Soc. Chim. Fr.*, 1906 (1968).
27. Tewari, P. H., Hunt, A. J., and Lofftus, K. D., *Mater. Lett.* **3,** 363 (1985).
28. Woignier, T., Ph.D. thesis, Université des Sciences et Techniques du Languedoc, Montpellier, France, 1984.
29. Iacobucci, P. A., Cheng, C.-P., and Walsh, E. N., European Patent 0,186,149, December 19, 1985.
30. Livage, J., Henry, M., and Sanchez, C., *Prog. Solid State Chem.* **18,** 259 (1988).
31. Aizawa, M., Nosaka, Y., and Fujii, N., *J. Non-Cryst. Solids* **128,** 77 (1991).
32. Schutte, C. L., Fox, J. R., Boyer, R. D., and Uhlmann, D. R., *in* "Ultrastructure Processing of Advanced Materials" (D. R. Uhlmann and D. R. Ulrich, Eds.), p. 95. Wiley, New York, 1992.
33. Yoldas, B. E., *J. Non-Cryst. Solids* **38,** 81 (1980).
34. Lin, C. C., and Basil, J. D., *Mater. Res. Soc. Symp. Proc.* **73,** 585 (1986).
35. Basil, J. D., and Lin, C.-C., *in* "Ultrastructure Processing of Advanced Ceramics" (J. D. Mackenzie and D. R. Ulrich, Eds.), p. 783. Wiley, New York, 1988.
36. Basil, J. D., and Lin, C.-C., *Mater. Res. Soc. Symp. Proc.* **121,** 49 (1988).
37. Yamane, M., Inoue, S., and Yasumori, A., *J. Non-Cryst. Solids* **63,** 13 (1984).
38. Walther, K. L., Wokaun, A., Handy, B. E., and Baiker, A., *J. Non-Cryst. Solids* **134,** 47 (1991).
39. Schraml-Marth, M., Walther, K. L., Wokaun, A., Handy, B. E., and Baiker, A., *J. Non-Cryst. Solids* **143,** 93 (1992).
40. Bernards, T. N. M., van Bommel, M. J., and Boonstra, A. H., *J. Non-Cryst. Solids* **134,** 1 (1991).
41. Hutter, R., Mallat, T., and Baiker, A., *J. Catal.* **153,** 177–189 (1995).
42. Thermodynamics Research Center, The Texas A&M University System, *in* "TRC Thermodynamic Tables—Non-Hydrocarbons," Vol. IV, p. i-5000. College Station, Texas 1992.
43. Barrett, E. P., Joyner, L. G., and Halenda, P. P., *J. Am. Chem. Soc.* **73,** 373 (1951).
44. Broekoff, J. C. P., *in* "Preparation of Heterogeneous Catalyst II" (B. Delmon, P. Grange, P. Jacobs, and G. Poncelet, Eds.), p. 663. Elsevier, Amsterdam, 1979.
45. Harkins, W. D., and Jura, G., *J. Chem. Phys.* **11,** 431 (1943).
46. Klug, H. P., and Alexander, L. E., "X-Ray Diffraction Procedures for Polycrystalline and Amorphous Materials." Wiley, New York, 1974.
47. JCPDS Mineral Powder Diffraction Data File 21-1272, Park Lane, Pennsylvania.
48. Mukherjee, S. P., *J. Non-Cryst. Solids* **42,** 477 (1980).
49. Bihuniak, P. P., and Condrate, R. A., *J. Non-Cryst. Solids* **44,** 331 (1981).
50. Best, M. F., and Condrate, R. A., *J. Mater. Sci. Lett.* **4,** 994 (1985).
51. Salvado, I. M. M., and Navarro, J. M. F., *J. Non-Cryst. Solids* **147&148,** 256 (1992).
52. Bräutigam, U., Meyer, K., and Bürger, H., *in* "EUROGEL '91" (S. Vilminot, R. Nass, and H. Schmidt, Eds.), p. 335. Elsevier, Amsterdam, 1992.
53. Duran, A., Serna, C., Fornes, V., and Fernandez-Navarro, J. M., *J. Non-Cryst. Solids* **82,** 69 (1986).
54. Sing, K. S. W., Everett, D. H., Haul, R. A. W., Moscou, L., Pierotti, R. A., Rouquérol, J., and Siemieniewska, T., *Pure Appl. Chem.* **57,** 603 (1985).
55. Bertoluzza, A., Fagnano, C., Morelli, M. A., Gottardi, V., and Guglielmi, M., *J. Non-Cryst. Solids* **48,** 117 (1982).
56. Schneider, M., "Titania Based Aerogel Catalysts," Diss. ETH No 10685, Swiss Federal Institute of Technology, Zurich, 1994.
57. Rangarajan, B., and Lira, C. T., *Mater. Res. Soc. Symp. Proc.* **271,** 559 (1992).
58. Overbury, S. H., Bertrand, P. A., and Somorjai, G. A., *Chem. Rev.* **75**(5), 547 (1975).
59. Schneider, M., and Baiker, A., *in* "Encyclopedia of Advanced Materials" (D. Bloor, R. J. Brook, M. C. Flemings, and S. Mahajan, Eds.), Vol. 1. Pergamon Press, Oxford, 1994.
60. Perry, C. C., and Li, X., *in* "Chemical Processing of Advanced Materials" (L. L. Hench and J. K. West, Eds.), p. 131. Wiley, New York, 1992.
61. Meyer, E., Zanotto, E. D., and Aegerter, M. A., *J. Non-Cryst. Solids* **121,** 279 (1990).
62. Zanotto, E. D., *J. Non-Cryst. Solids* **147&148,** 820 (1992).
63. Ingo, G. M., Dirè, S., and Babonneau, F., *Appl. Surf. Sci.* **70/71,** 230 (1993).
64. Yamane, M., Aso, S., Okano, S., and Sakaino, T., *J. Mater. Sci.* **14,** 607 (1979).